Microscopy and Microanalysis, **29** (Suppl 1), 2023, 961–963
https://doi.org/10.1093/micmic/ozad067.480

Microscopy AND Microanalysis

Meeting-report

Towards the Visual Proteomics of *C. reinhardtii* using High-throughput Collaborative *in situ* Cryo-ET

Sagar Khavnekar[1], Ron Kelley[2], Florent Waltz[3], Wojciech Wietrzynski[3], Xianjun Zhang[2], Martin Obr[2], Grigory Tagiltsev[4], Florian Beck[1], William Wan[5], John Briggs[4], Ben Engel[3], Juergen Plitzko[1], and Abhay Kotecha[2,*]

[1]*Cryo-EM Technology group, Max Planck Institute of Biochemistry, Martinsried, Germany*
[2]*Thermo Fisher Scientific, Eindhoven, The Netherlands*
[3]*Biozentrum, University of Basel, Basel, Switzerland*
[4]*Department of Virus and Cell structure, Max Planck Institute of Biochemistry, Martinsried, Germany*
[5]*Vanderbilt University, Nashville, USA*

*Corresponding Author: abhay.kotecha@thermofisher.com

Cryo-electron tomography (cryo-ET) is emerging as the method of choice for determining the structures of biological macromolecules *in situ*, that is, within their native context inside cells or extracellular particles. In recent years, cryo-ET and subsequent subtomogram averaging of large macromolecular complexes with molecular weights on the order of megadaltons have produced structures at resolutions sufficient to visualize sidechains (3-5Å) [1-3]. These specimens have typically been cryo-fixed in vitrified ice 200nm or thinner. Thicker vitrified single cells and, more recently, tissues from multicellular organisms have been micromachined using Gallium cryo-focused ion beam (Ga^+-cryo-FIB milling) to produce electron transparent sections with thicknesses of 200 nanometres or less; these sections are referred to as lamellae. Despite being sufficiently thin, subtomogram averages of macromolecular complexes within these cryo-FIB milled lamellae have often been limited to resolutions lower than 10 Å [4,5]. These resolution limitations were likely due to poor lamella quality owning to redeposition and beam induced motion due to charging during tilt-series data acquisition, as recent improvements in Ga^+-cryo-FIB hardware and protocols have enabled subtomogram averaging of macromolecular structures at sub-5 Å resolutions [6,7]. Furthermore, current Ga^+-cryo-FIB systems suffer from low throughput due to manual sample transfers and Ga^+ ion beam damage [8]. A next-generation cryo-FIB that uses plasma instead of Gallium (cryo-plasmaFIB), from Thermo Fisher Scientific reduces redeposition and ion beam damage while improving the throughput with automated sample transfers [9]. Combined with recent advances in automation of tilt-series data acquisition [10-12], it is now possible to collect large in situ cryo-ET datasets on lamellae of cells and tissues to determine high-resolution molecular atlases, i.e., visual proteomics.

In order to benchmark the performance of the cryo-plasmaFIB, we used *S. cerevisiae* as an established model system[7]. Preliminary benchmarks resulted in 6.5 Å subtomogram average of 80S ribosomes from 7 tomograms acquired on a single lamella, cryo-FIB milled using Xenon plasma (Figure 1A). In addition to negligible redeposition, increased throughput from automated transfers allowed for faster screening, leading to a large dataset. Upon analysis of the whole dataset containing 260 tomograms (119k subvolumes), we were able to obtain a sub-5 Å subtomogram average of the large subunit with local resolution extending to the Nyquist resolution (3.9Å) (Figure 1B). Our analysis of Rosenthal-Henderson B-factors of 80S ribosomes from lamellae with varying thicknesses demonstrates an inverse relationship between specimen thickness and signal-to-noise ratio (SNR) (Figure 1C). While this may suggest that it is beneficial to micromachine thinner lamellae, further analysis of Rosenthal-Henderson B-factors for 80S ribosomes at varying depth within lamellae indicates approximately 30 nanometre (nm) damage layer (Figure 1D). These benchmark results demonstrate the potential of newly developed cryo-plasmaFIB for high-throughput and high-resolution cellular cryo-ET to realise visual proteomics approaches.

As a proof of principle of such approaches, we are currently generating a large in situ cryo-ET dataset containing thousands of tomograms from *C. reinhardtii*. *C. reinhardtii* offers a well-established model system to study many fundamental cellular processes (Figure 2A) and has impacted our understanding of human diseases [13]. However, prior studies to map macromolecular complexes in *C. reinhardtii* were limited to lower resolution (> 10 Å) subtomogram averages [4,14]. In addition, smaller dataset size and need to average a large number of subvolumes limited subtomogram averaging of low copy number macromolecular complexes. Building on our benchmark results with *S. cerevisiae*, we present preliminary results for C. *reinhardtii*, showing that we are able to obtain *in situ* sub-nanometre subtomogram averages of biomolecular complexes ranging in size from megadaltons to several hundred kilodaltons. Using just 6 tomograms acquired on a single lamella, we obtained a 6 Å subtomogram average of 80S ribosomes (Figure 2A). In addition, we present a 7 Å subtomogram average of RuBisCO (~ 520 kilodaltons) within the pyrenoid (Figure 2B-C), a phase separated and crowded compartment (Figure 2D). To our knowledge, it represents one of the first subnanometre subtomogram average of a macromolecule in native phase separated environment. These results, combined with higher throughput, establish a proof of principle to obtain subnanometre subtomogram average of low-copy number macromolecules and hence, to feasibility to determine the Visual Proteome of *C. reinhardtii*.

However, one is challenged by an increasing number of unknown and known macromolecular complexes in such large datasets (Figure 2E). This limits individual efforts to identify, average, classify, and curate macromolecular complexes and prompts for a collaborative effort. We envision that our collaborative efforts to curate all macromolecular complexes using a large open access dataset will offer invaluable insights into the molecular functioning of fundamental cellular processes. Furthermore, the availability of such large curated molecular atlases will prove to be instrumental in the development of new computational tools for *in situ* cryo-ET.

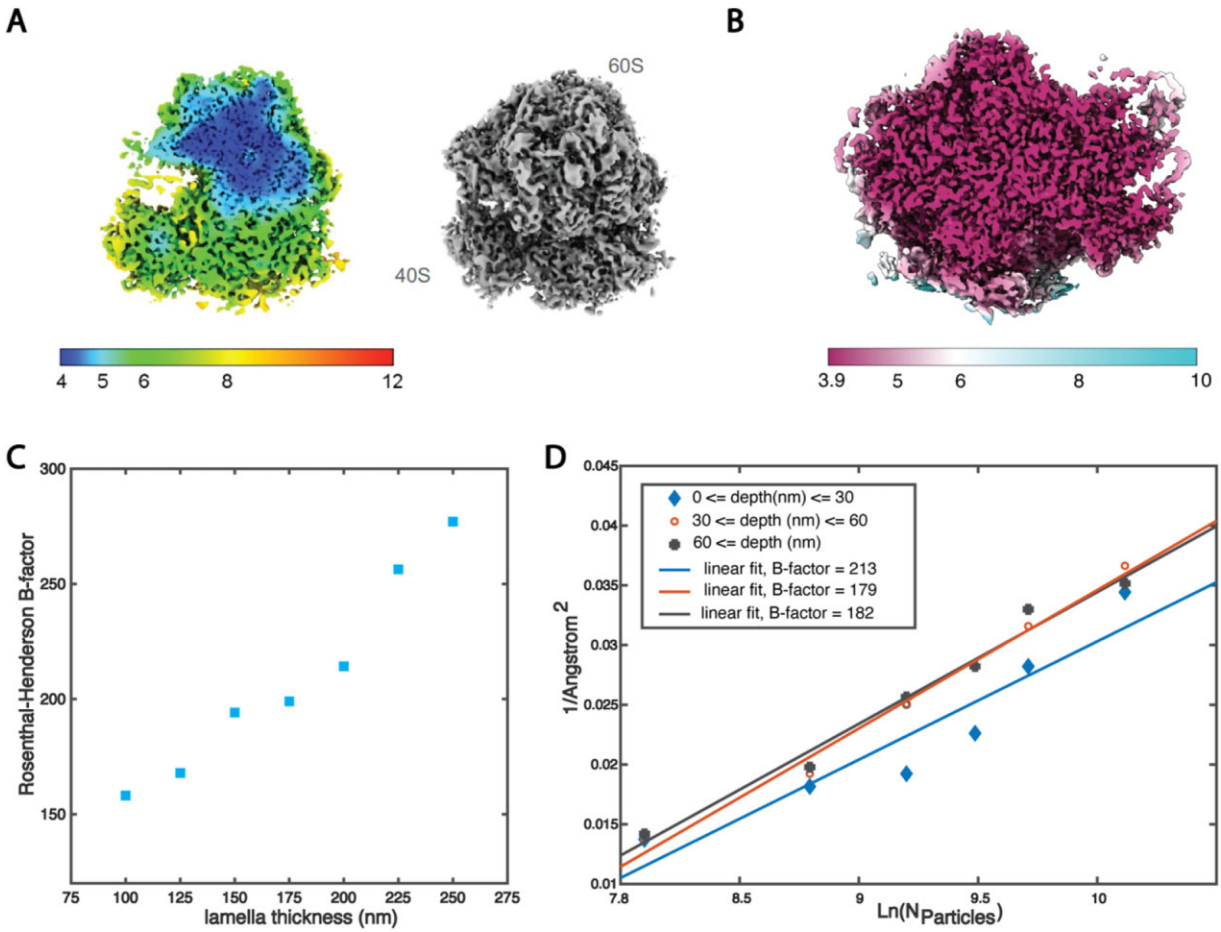

Fig. 1. Benchmarking the performance of prototype cryo-plasmaFIB with *S. cerevisiae*. (A) 80S ribosome subtomogram average from a single lamella (7 tomograms). Local resolution scale in Å. (B) Large subunit (60S) subtomogram average (focused alignment) demonstrating Nyquist resolution (3.9Å) in most parts. Subtomogram average obtained from 260 tomograms. Local resolution scale in Å. (C) Rosenthal-Henderson B-factors at increasing tomogram thicknesses (each point accommodates thickness within range ±25nm). (D) Rosenthal-Henderson B-factor plot at varying depths (in nanometre) from lamellae surface.

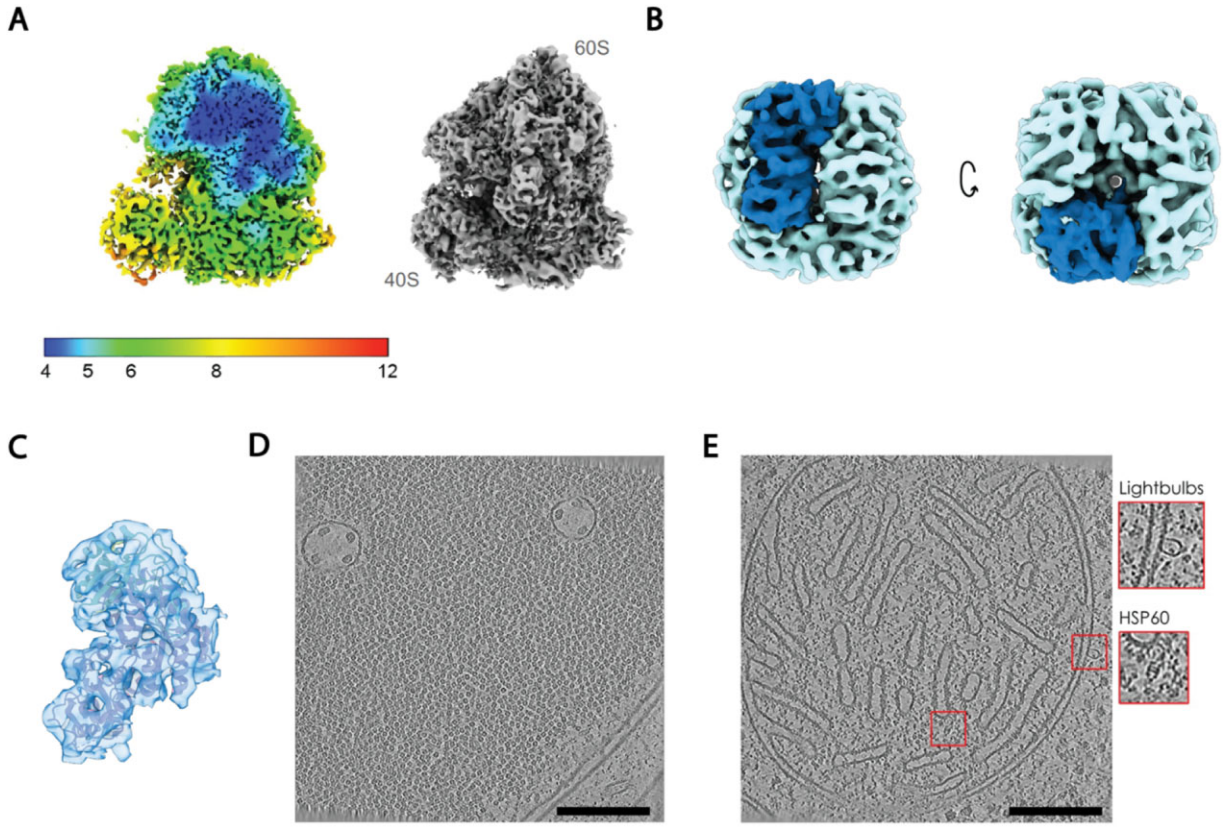

Fig. 2. Towards the Visual Proteomics of *C. reinhardtii* using high-throughput collaborative in situ cryo-ET (A) 80S ribosome subtomogram average from a single lamella (6 tomograms). Local resolution scale in Å. (B) ~7 Å subtomogram average of RuBisCO and (C) a rigid body fit of an atomic model of RuBisCO to structural asymmetric unit highlighted in (B). (D) Representative tomogram showing Pyrenoid, a phase separated compartment of RuBisCO. (E) Representative tomogram highlighting known (e.g., HSP60-HSP10 chaperonin) and unknown (e.g., Lightbulbs) macromolecular complexes associated with mitochondria. Scale bars 200nm.

References

1. FKM Schur *et al.*, *Science* **353**(1979) (2016), p. 506.
2. D Tegunov *et al.*, *Nat Methods* **18** (2021), p. 186.
3. L Xue *et al.*, *Nature* **610** (2022), p. 205.
4. S Albert *et al.*, *Proc Natl Acad Sci USA* **117** (2020), p. 1069.
5. PS Erdmann *et al.*, *Nature Communications* **12**(1) (2021), p. 1.
6. Z Wang *et al.*, *Science* **375**(1979) (2022), p. eabn1934.
7. S Khavnekar *et al.*, *BioRxiv* (2022) 2022.06.16.496417.
8. BA Lucas and N Grigorieff, *BioRxiv* (2023) 2023.02.01.526705.
9. C Berger *et al.*, *Nature Communications* **14**(1) (2023), p. 1.
10. J Bouvette *et al.*, *Nat Commun* **12** (2021), p. 1957.
11. F Eisenstein *et al.*, *Nat Methods* **20** (2023), p. 131.
12. S Khavnekar *et al.*, *J Struct Biol* **215** (2023), p. 107911.
13. EH Harris, *Annu Rev Plant Physiol Plant Mol Biol* **52** (2001), p. 363.
14. BD Engel *et al.*, *Elife* **4** (2015), p. e04889.